Effects of Geological Structures on Rainfall-Runoff Responses in Headwater Catchments in a Sedimentary Rock Mountain

Running head:
Effects of Geological Structures on Rainfall-Runoff Responses

Authors:
Jun Inaoka, Ken'ichirou Kosugi, Naoya Masaoka, Tetsushi Itokazu*, & Kimihito Nakamura
Graduate School of Agricultural Sciences, Kyoto University, Kyoto, Kyoto, Japan
*Present address: Faculty of Law, Economics and Management, Okinawa University, Naha, Okinawa, Japan

Corresponding Author:
Jun Inaoka
inaoka.jun.63c@st.kyoto-u.ac.jp

Keywords:
Sedimentary rock mountains; rainfall-runoff responses; geological structures; dips; strikes; slope angle; flow direction; hydraulic anisotropy

Acknowledgments:
We thank Ministry of Land, Infrastructure and Transport, Japan, for providing the topographic data. This work was partly supported by JST, CREST, and the Fund of Monbukagakusho for Scientific Research (20H00434).

Data Availability Statement:
Research data are not shared.

Effects of Geological Structures on Rainfall-Runoff Responses

Abstract

Clarifying rainfall-runoff responses in mountainous areas is essential for disaster prediction as well as water resource management. Although runoff is considered to be significantly affected by topography, some previous studies have reported that geological structures also have significant effects on rainfall-runoff characteristics. Particularly in headwater catchments located in sedimentary rock mountains, dips and strikes may significantly affect rainwater discharge. In this study, the effects of geological structures on rainfall-runoff characteristics were investigated based on observed discharge hydrographs from twelve catchments, which lie radially from the summit of a sedimentary rock mountain. The results obtained were as follows: (1) Even though the topographic wetness index (TWI) distributions of the twelve catchments were similar, there were significant differences in their runoff characteristics; (2) Catchments with average flow direction oriented toward the strike direction (strike-oriented catchments) are characterized by large baseflows; (3) Catchments with average flow direction oriented toward the opposite dip direction (opposite dip-oriented catchments) are steep, and this results in quick storm runoff generation; (4) Catchments with average flow direction oriented toward the dip direction (dip-oriented catchments) are gentle, and this results in delayed storm runoff generation. It was presumed that in strike-oriented catchments, large quantities of groundwater flowing along the bedding planes owing to hydraulic anisotropy, exfiltrate and sustain the large amount of the observed baseflow, i.e., in strike-oriented catchments, runoff is directly controlled by geological structures. Conversely, in opposite dip-oriented and dip-oriented catchments, runoff is indirectly controlled by geological structures, i.e., geological structures affect slope gradients, which result in differences in storm runoff generation. Thus, this study clearly illustrates that geological structures significantly affect rainfall-runoff responses in headwater catchments located in sedimentary rock mountains.

INTRODUCTION

Japan has been subject to several disasters (Okada, Ye, Kajitani, Shi, & Tatano, 2011; Ushiyama, Honma, Yokomaku, & Sugimura, 2019), including slope failures, debris flows, and landslides (Marutani *et al.*, 2017; Miyagi *et al.*, 2011), and adequate preparation for these hazards is still a major challenge. To accurately predict sediment disasters, an understanding of rainfall-runoff responses in mountainous areas is important (Corominas, Moya, Ledesma, Lloret, & Gili, 2005; Kosugi *et al.*, 2011). Additionally, rainfall-runoff responses do not only affect sediment disasters, they also affect flood prediction (Fujimoto, Ohte, & Tani, 2008), water resource management (Hughes, 1995), and chemical as well as ecological material transport (Sakai, Munakata, & Kimura, 2009). Thus, studying on rainfall-runoff responses is enormously beneficial to the society.

In previous studies, the effects of vegetation and land use on rainfall-runoff responses have been reported (Kirkby, Bracken, & Reaney, 2002; Tani *et al.*, 2012). Additionally, it has been reported that topography and geology affect rainfall-runoff responses (Iwashita, Onda, & Ichiyanagi, 1994; Kato *et al.*, 2000; Tani *et al.*, 2012), and that the effect of topography is very significant (Beven & Kirkby, 1979; Hernandez, Nachabe, Ross, & Obeysekera, 2003; Zevenbergen & Throne, 1987), i.e., large catchment areas tend to develop overland saturated flow; thus, they significantly result in an increase in runoff. Gentle topographic slopes also tend to develop overland saturated flow given that groundwater movements become slower. Furthermore, the steep channel gradient contributes to rapid runoff. Based on these topographical effects, Beven and Kirkby (1979) developed TOPMODEL, and it is one of the most widely used hydrological models today. However, many previous studies in which the effects of topography on rainfall-runoff responses were investigated did not consider the effects of geological structures.

Studies on the effects of geological structures on rainfall-runoff responses have been primarily conducted in crystalline mountains (*e.g.,* Fujimoto *et al.*, 2008; Han, Yang, Fan, Xiao, & Moiwo, 2012; Miyata, Uchida, Asano, Ando, & Mizuyama, 2003; Séguis *et al.*, 2011). However, in some previous studies, the focus was on catchments in sedimentary rock mountains (Komatsu, 2008; López-Tarazón, Batalla, Vericat, & Balasch, 2010; Uchida, Kosugi, & Mizuyama, 1999). Moreover, Kato *et al.* (2000) and Tani *et al.* (2012) compared catchments in crystalline and sedimentary rock mountains. However, the exact effects of dips and strikes, which are typical of sedimentary rock mountains, on rainfall-runoff responses have not yet been evaluated.

Dips and strikes, which are not characteristic of crystalline rocks that are formed from the solidification of magma, are features that develop during the formation of sedimentary rocks. Therefore, to study rainfall-runoff responses in sedimentary rock mountains, the results obtained for crystalline rock mountains cannot be applied. Additionally, it is necessary to evaluate the effects of geological structures that are characterized by dips and strikes on rainfall-runoff responses. Actually, Kato *et al.* (2000) observed that catchments located in sedimentary rock mountains show greater variations in rainfall-runoff responses than those located in crystalline mountains.

In sedimentary rocks, different rock layers share a bedding plane creating hydraulic anisotropy (Singhal & Gupta, 2010). Thus, it has been reported that, in sedimentary rocks, a greater amount of water tends to infiltrate parallel to the bedding plane than in the orthogonal direction (Suenaga, Kiho, & Okada, 2002). Such effect of hydraulic anisotropy can be found in other geological settings. For example, Jefferson, Grant and Rose (2006) discussed the hydraulic anisotropy caused by lava flow geometry through the volcanic history. They studied discharges, temperatures, and water chemistries of seven springs located in the west of the Oregon High Cascades, which showed the effects of geological stratigraphy on runoff. Thus, the groundwater system can significantly be affected by the hydraulic anisotropy originated from geological stratigraphy.

In sedimentary rock mountains, previous studies suggested convergence of groundwater flows in the direction of strikes. For example, Sakai *et al.* (2009) monitored the spatial distribution of baseflow discharge from catchments with an area of a few km^2 located in the Plio-Pleistocene Kazusa Group in Boso Peninsula, Japan. They also revealed that catchments that have average flow direction oriented toward the strike (*i.e.,* strike-oriented catchments) tended to have large baseflows. Strike-oriented groundwater movements are also reported in the results of a study conducted in pre-glacial Canadian Rocky Mountains (Ford, 1983). However, in these previous studies, the effects of dips and strikes on rainfall-runoff responses in headwater catchments, which are the most important source regions for runoff generation, were not investigated, and none of these previous studies focused on the effects of geological structures on storm runoff responses. Additionally, the runoff properties of catchments that have their average flow direction oriented toward the dip direction (*i.e.,* dip-oriented catchments) and toward the opposite dip direction (*i.e.,* opposite dip-oriented catchments), have not yet been clarified.

Therefore, the objective of this study was to evaluate the effects of geological structures on rainfall-runoff responses in headwater catchments in sedimentary rock mountains. Based on the simultaneous observation of twelve catchments that lie radially from a single, isolated mountain peak, this study aims to clarify the effects of dips and strikes, which characterize sedimentary rock mountains, on water discharge.

METHODS

Study site

The study was conducted in the Shigaraki Experimental Forest, which is located in the Southern Shiga Prefecture, central Japan (Figure 1a). During the study, rainwater discharges from twelve catchments that extend radially from the peak of Mt. Kanayama, which is located at the center of the experimental forest, and is 565.2 m above sea level, were investigated (Figure 1b). Between 1981 and 2010, the mean annual precipitation and mean annual temperature measured at the Shigaraki Station of the Japan Meteorological Agency, which is located 9.8 km northeast of the study site, were 1466.1 mm and 12.2°C, respectively. As shown in Figure 2, the geology of the study area is a melange matrix of mudstone and sandstone, partially containing chert, accreted in the Jurassic period (Wakita *et al.*, 2013). In sedimentary rock mountains, the strata have slope and direction called dips and strikes (Figure 3). Based on Figure 2, which shows the results of a study conducted by Wakita *et al.* (2013), and our survey, the strikes in this study area have direction in the range N 48° E to N 139.5° E, with a mean of N 101.6° E, while the dips have direction in the range 25° N to 85° N, with a mean of 55° N (Table I). The vegetation of the study area is a planted forest, primarily consisting of *Chamaecyparis obtusa* (Japanese cypress) and *Cryptomeria japonica* (Japanese cedar), which were both planted in the 1950s (Tani *et al.*, 2012). Every catchment in this study area is covered with brown forest soil (Tani *et al.*, 2012), which is typical of low relief mountains in Japan.

Observation methods

Runoff was observed at the outlets of the twelve catchments shown in Figure 1(b). The twelve catchments were numbered based on their clockwise locations (*i.e.*, catchments S01–S12), and the areas of the twelve catchments as well as their average slopes are summarized in Table II. A V-notch weir made of stainless steel and a water level sensor was installed in the outlet of each catchment, and water level was recorded using a data-logger (HIOKI LR5042) at five-minute intervals. The angle of the V-notch weir is 90° for every catchment, except for the S02 and S10 catchments. For the S02 and S10 catchments, a V-notch weir with an angle of 60° was used. Precipitation was observed at an open space close to catchment S04 using a tipping-bucket rain gauge with a resolution of 0.5 mm (Figure 1b).

Storm events

In this study, two storm events, both of which resulted in a total rainfall of ~60 mm, were analyzed (Table III). Prior to each of these events, there was a long no-precipitation period. Moreover, both events had relatively simple hyetographs. As shown in Table III, event 1 had a greater peak intensity than event 2.

Analyses of hydrographs

For calculating direct runoff, we used the same method employed by Hewlett and Hibbert (1967), which allows the separation of the hydrograph into direct runoff and baseflow using a straight line unique to watershed. To separate the hydrographs of all the catchments, a line with a constant slope value of 2.4×10^{-5} mm/h/h was assumed.

For analyzing storm runoff timing, we computed D_1 and D_2 values. Here, D_1 represents the direct runoff amount during the period from the start to the end of precipitation, and D_2 represents the direct runoff amount 24 h just after the precipitation ceased. The ratio of D_2 to D_1 represents the timing of storm runoff occurrence.

Calculation of the area-proportional discharge ratio and the observed discharge ratio

To evaluate the characteristics of the hydrographs observed in detail, the following method, which allows the comparison of the area-proportional discharge ratio and the observed discharge ratio for each catchment, was used.

Primarily, the total discharge from the mountain, Q_{all} [$\mathrm{L^3T^{-1}}$], was defined as:

$$Q_{\mathrm{all}} \equiv \Sigma Q_i \qquad (1)$$

where Q_i represents the discharge from each catchment, i, and the summation involved all twelve catchments. Additionally, the total catchment area of the mountain, $\mathrm{A_{all}}$ [$\mathrm{L^2}$] was defined as:

$$\mathrm{A_{all}} \equiv \Sigma \mathrm{A}_i \qquad (2)$$

where A_i represents the area of each catchment, i. Thus, the total specific discharge, q_{all} [$\mathrm{LT^{-1}}$], from the mountain was calculated as:

$$q_{\mathrm{all}} = Q_{\mathrm{all}}/\mathrm{A_{all}} \qquad (3)$$

In contrast, the specific discharge from each catchment, i, denoted q_i, was calculated as:

$$q_i = Q_i/\mathrm{A}_i \qquad (4)$$

On the other hand, the area-proportional discharge, Q_i' (*i.e.,* the discharge expected from each catchment based on its area) was then calculated according to Equation (5) below.

$$Q_i' = Q_{\mathrm{all}}\mathrm{A}_i/\mathrm{A_{all}} \qquad (5)$$

where $Q_i^{'}$ represents the area-proportional discharge from each catchment, i. Equation (5) indicates that the ratio of the area-proportional discharge from each catchment, i, to the total discharge from the mountain (*i.e.,* the area-proportional discharge ratio for catchment i) is the same as the ratio of the area of catchment i to the total catchment area of the mountain, A_i^*, i.e.,

$$Q_i^{'}/Q_{all} = A_i/A_{all} \equiv A_i^* \qquad (6)$$

In contrast, the ratio of the observed discharge from catchment i to the total discharge from the mountain (*i.e.,* the observed discharge ratio for catchment i), Q_i^*, was calculated as:

$$Q_i^* = Q_i/Q_{all} \qquad (7)$$

Substituting Equations (3) and (4) into Equation (7) gave:

$$Q_i^* = A_i^* q_i/q_{all} \qquad (8)$$

By comparing the area-proportional discharge ratio, A_i^*, and the observed discharge ratio, Q_i^*, it was possible to evaluate the contribution of each catchment to the total discharge from the mountain, i.e., when Q_i^* was greater than A_i^*, it implied that the discharge yield of the catchment, i, was greater than the discharge expected from the catchment area, and when Q_i^* was less than A_i^*, it implied that the yield discharge of the catchment, i, was lower than expected value. Equation (8) shows that Q_i^* is greater than A_i^* when q_i is greater than q_{all}. If the q_i hydrograph is the same as the q_{all} hydrograph, then Q_i^* will always be equal to the constant, A_i^*.

Terrain analysis

To evaluate the topography of each catchment, the distribution of the topographic wetness index (TWI) introduced by Beven and Kirkby (1979) was determined. TWI is a fundamental variable in TOPMODEL, which was developed by Beven and Kirkby (1979), and it is indicative of the development of saturation-excess overland flow. When a catchment is cut into grids, the TWI value of each grid can be calculated based on the ratio of the upslope area to the tangent of the topographical slope of the grid. In this study, we used SAGA plugins from QGIS (ver. 3.4.12) (QGIS Development Team, 2019) to calculate TWI values using the one-meter mesh digital elevation model (DEM) developed by the Ministry of Land, Infrastructure, Transport, and Tourism (MLIT), Japan.

RESULTS

Observed hydrographs

The results obtained after monitoring the runoff and precipitation events are shown in Figure 4, which reveal that even though all the catchments are located in the same mountain, their runoff characteristics were significantly different. For example, the peak runoff of catchment S06 was very high, while that of catchment S01 was relatively lower, and catchments S03 and S09 had very high baseflows. Additionally, these observations were similar for both storm events. For event 1, which showed a high first precipitation peak and low second precipitation peak (Figure 4), all the catchments, excluding catchments S10 and S11, had a peak runoff corresponding to the first precipitation peak. On the other hand, catchments S10 and S11 had peak runoffs corresponding to the second precipitation peak. For event 2, the hydrograph of catchment S12 clearly showed a delayed second peak after the precipitation event ceased.

Characteristics of hydrographs

Figure 5(a) shows a comparison of the runoff for a duration of one hour prior to the start of each event for the different catchments. These runoff data can be regarded as baseflows, since there was a long no-rainfall period preceding each event (Table III). From this figure, it is evident that catchments S03 and S09, which are located eastward and westward of the mountain summit respectively, had remarkably high baseflow runoffs before both storm events. Among the other catchments, catchments S02 and S07 showed relatively high baseflow runoffs, while the baseflow runoff of catchment S10 was the lowest.

In Figure 5(b), the storm peak flow rates (*i.e.*, the maximal one hour runoff for each event) of the different catchments are compared. The southern catchments, S06 and S07, showed high storm peak flow rates, while the northern catchments, S12 and S01, showed lower values.

Figure 5(c) shows that the trends observed in the direct runoff distribution were similar to those in the storm peak flow distribution shown in Figure 5(b), i.e., catchments S06 and S07 had high direct runoffs, while the direct runoffs of catchments S01 and S12 were generally lower. However, the differences in direct runoffs of all the catchments were less distinct than the differences in their peak flow rates. Particularly, in catchment S12, the direct runoff for event 2 was much higher than that for event 1, and this was attributed to be the occurrence of the second peak in catchment S12 as shown in Figure 4.

The observation that event 2 resulted in a much greater direct runoff than event 1 was also true for catchment S10. For the other catchments, the direct runoff for event 2 was also higher than for event 1. Figure 5(a) indicates that the baseflow rate before event 2 was higher than that before event 1 for most of the catchments, and as shown in Table III, event 2 had a shorter anteceding no-precipitation period than event 1. Additionally, Suzuki (1980) suggested that the non-rainfall period before event 2 (*i.e.,* early October) showed a lower potential evapotranspiration than that before event 1 (*i.e.,* mid-September). These observations suggest a wetter anteceding condition for event 2 than for event 1, which probably resulted in the higher direct runoff for event 2.

Figure 5(d) compares the ratio D_2 to D_1, which represents the timing of storm runoff occurrence. A high D_2 to D_1 ratio implied a delayed occurrence of the storm runoff. For event 1, the ratio was high for catchments S10 and S11, and for event 2, it was high for catchments S10, S11, S12, and S01, indicating that catchments located northwestward, northward, and northeastward to the mountain summit tended to show delayed storm runoff timings.

Catchment classification based on the observed discharge ratio

The specific discharges that were used to compute the observed discharge ratio are summarized in Figure 6(a), and Figure 6(b) shows the area-proportional discharge ratio, A_i^*, and the observed discharge ratio, Q_i^*, for catchments S03, S06, and S12 during event 2. These catchments exhibited distinctive Q_i^* hydrographs.

As shown in Figure 6(b), catchment S03 showed a very high Q_{S03}^* compared to A_{S03}^* before precipitation, i.e., the observed baseflow for catchment S03 was much larger than the value expected from the catchment area. During precipitation, Q_{S03}^* quickly decreases, and became approximately the same as A_{S03}^*, meaning that the storm runoff rate of catchment S03 is consistent with the explanation of the rate based on its area. After precipitation ceased, Q_{S03}^* gradually increased.

For catchment S06, the value of Q_{S06}^* was less than A_{S06}^* before precipitation, i.e., catchment S06 has smaller baseflow than expected from its area. During precipitation, Q_{S06}^* increased significantly, and formed a sharp peak at approximately the same time as the precipitation peak, at which it was more than two-fold as high as A_{S06}^*. After precipitation, it decreased immediately, and became lower than A_{S06}^*. Thus, the storm flow from catchment S06 responded quickly to precipitation input, compared with the total storm flow response of the mountain.

Like Q_{S06}^*, the value of Q_{S12}^* was less than A_{S12}^* before precipitation, indicating the small baseflow of catchment S12 for its area. During precipitation, there was no significant increase in Q_{S12}^*, suggesting that the runoff from catchment S12 remained below the expected value. However, close to the end of precipitation, Q_{S12}^* began to increase, and after precipitation, it formed a dull peak that lasted for a day, and thereafter declined gradually. In the vicinity of the peak, Q_{S12}^* became higher than A_{S12}^*, suggesting the occurrence of a discharge that was greater than the expected value. In summary, relative to the total storm flow from the mountain, the generation of storm flow in catchment S12 was delayed.

Figure 7, which shows A_i^* and Q_i^* values for event 2 for all the catchments, clearly reveals that Q_{S09}^* was very similar to Q_{S03}^*; and that Q_{S09}^* had high values before the storm event, which decreased during precipitation and gradually increased again after the storm event. Thus, catchments S03 and S09 could be classified under the same group, characterized by a large baseflow (LBF). Figure 7 also shows that with the exception of catchments S03 and S09, all the other catchments had Q_i^* values that were smaller than their corresponding A_i^* values before the storm event, which means that they have smaller baseflow than LBF catchments.

The time series of both Q_{S05}^* and Q_{S07}^* were similar to that of Q_{S06}^*, i.e., they exhibit sharp peaks corresponding to the precipitation peak. Therefore, catchments S05, S06, and S07 could be classified under the same group, i.e., catchments characterized by relatively quick storm flow (QSF) occurrences. Moreover, even though Q_{S04}^* gradually increased after precipitation, it showed a sharp peak that corresponded to the precipitation peak, and even though the peak of Q_{S08}^* was relatively dull and small, it appeared at approximately the same time as the precipitation peak. Thus, it was reasonable to classify both S04 and S08 catchments into the quasi-QSF group.

The values of Q_{S11}^* and Q_{S10}^* shown in Figure 7 were similar to that of Q_{S12}^*. Given that catchments S10 and S11 both showed dull peaks after precipitation ceased, together with catchments S12, they were classified into the same group, i.e., catchments characterized by relatively delayed storm flow (DSF) occurrences. Moreover, even though Q_{S01}^* and Q_{S02}^* varied slightly during precipitation, they were each characterized by a dull peak after the precipitation peak. Therefore, catchments S01 and S02 were classified under the quasi-DSF group.

Figure S1 shows the variation of the computed Q_i^* during event 1 for all the catchments. The trends shown in this figure are approximately the same as those shown in Figure 7 for event 2, indicating that the classification of catchments based on runoff characteristics is consistent for both storm events. Thus, in the vicinity of Mt. Kanayama, the twelve catchments were classified into the three groups: catchments with large baseflow (LBF: S03, S09), catchments with relatively quick storm flow (QSF: S05, S06, S07, and quasi-QSF: S04, S08), and catchments with relatively delayed storm flow (DSF: S10, S11, S12, and quasi-DSF: S01, S02).

DISCUSSION

Relation between geological characteristics and runoff characteristics

As shown in Figures 7 and S1, catchment classification based on runoff characteristics seems greatly related with catchment direction from the summit of Mt. Kanayama, suggesting that rainfall-runoff responses might be controlled by the flow directions of the catchments. To confirm this suggestion, the flow directions of each of the twelve catchments were computed using the method proposed by Sakai *et al.* (2009), who defined flow direction as the direction from the highest to the lowest point (*i.e.,* the outlet) of the catchment. The resulting flow directions for catchments S03 and S09, both of which were categorized as LBF catchments (Figures 7 and S1), were N80° E and N84° W, respectively, and both of them were oriented northward by 8° from the N88° E line (Figure 8). Based on this N88° E line, the flow direction was defined by an angle, θ, as shown in Figure 8, and the sin θ values for all the catchments were compared. For example, given the flow direction of catchment S12 (N8° E) as shown in Figure 8, its computed θ was 80°, and the resulting sin θ was 0.98.

A summary of the sin θ values of all the catchments is shown in Figure 9, which clearly shows that the sin θ values corresponded well to the classification of the catchments based on runoff characteristics. LBF catchments (*i.e.,* the S03 and S09 catchments) had a sin θ value of 0.14, while QSF and quasi-QSF catchments had negative sin θ values ranging from –0.93 to –0.68, and DSF and quasi-DSF catchments had large sin θ values ranging from 0.21 to 0.98.

To evaluate the geological implication of the N88° E line, which was used to calculate the sin θ values, the N88° E line and the direction with sin θ value equal to 1 as well as the results of the dip and strike survey conducted by Wakita *et al.* (2013) were compared in Figure 2. The figure revealed that the N88° E line was approximately the same as the strike line in the vicinity of Mt. Kanayama, and the direction with sin θ = 1 corresponded to the dip direction. Therefore, the sin θ values shown in Figure 9 could be recognized as an index that can be used to evaluate the level of agreement between the flow direction of a catchment and the dip direction, i.e., when a catchment has a sin θ value close to 1, it implies that its flow direction is oriented toward the dip direction (*i.e.,* it is a dip-oriented catchment). Conversely, when the sin θ value of a catchment is close to zero, it implies that its flow direction is oriented toward the strike direction (*i.e.,* it is a strike-oriented catchment). Additionally, when the sin θ value is negative and close to -1, it implies that the flow direction of the catchment is oriented toward the opposite dip direction (*i.e.,* it is a opposite dip-oriented catchment). Therefore, the results shown in

Figure 9 indicate that the LBF, QSF, and DSF catchments corresponded to strike-oriented, opposite dip-oriented, and dip-oriented catchments, respectively.

Relations between the topographic index and runoff characteristics

In some previous studies, it has been reported that topography has a significant effect on rainfall-runoff responses (Hernandez *et al.*, 2003; Zevenbergen & Throne, 1987). Figure 10 shows the TWI distributions obtained for the 12 catchments studied, which revealed that the TWI distributions of all the catchments were similar. To evaluate the distributions of TWI objectively, we conducted two-sample Kolmogorov-Smirnov tests using the Matching package for R (Sekhon, 2011). According to the test, the maximum K-S statistic value was 0.2439 and the corresponding p-value was 0.136 implying that TWI distributions do not differ significantly. Thus, the surface topography characterized by the TWI distribution could not be used to describe the differences in the rainfall-runoff responses of the twelve catchments and had little to do with the classification of the catchments as LBF, QSF, or DSF.

The effect of geological structures on runoff

The strike-oriented catchments, S03 and S09, showed large amounts of baseflow, and were categorized as LBF catchments. In sedimentary rock mountains, a significant proportion of the baseflow results from the exfiltration of bedrock groundwater (Burns, Murdoch, Lawrence & Michel, 1998). According to Bruno (1994), Singhal and Gupta (2010), and Suenaga *et al.* (2002), sedimentary rocks, which are formed by the bonding of horizontally deposited materials, and consists of layers with different hydraulic conductivities, tends to have a higher permeability in the horizontal direction than in the vertical direction, i.e., sedimentary rocks show hydraulic anisotropy, characterized by a high hydraulic conductivity in the direction parallel to the bedding plane. Therefore, in sedimentary rock mountains, groundwater is expected to flow along the bedding plane. Figure 11 shows cross section image of the study site. As summarized in Table I, the average dip angle in the study site is 55°, which is greater than the average slope angle of the studied catchments (Table II). In Figure 11, rainwater infiltrated into the mountain would face the low hydraulic conductivity rock at some depths, and then flows downwards along the bedding plane forming the bedrock aquifer. Because the low hydraulic conductivity rock interrupts the water flow, only some parts of the bedrock aquifer can contribute to the exfiltration in the dip-oriented catchment and in the opposite dip-oriented catchment. In most parts of the aquifer, which are surrounded by the low hydraulic conductivity rocks, the only way for the water to exfiltrate is to flow toward the strike-oriented catchments. Thus, in the strike-oriented catchments, the large contribution of the bedrock aquifer sustains the significant baseflow.

Sakai *et al.* (2009) investigated baseflow discharges from basins with areas of a few km^2 in sedimentary rock mountains located in the Boso Peninsula, which is close to Tokyo, Japan. They analyzed rainfall-runoff responses in relation to geological structures and concluded that strike-oriented catchments tend to have large baseflows. Furthermore, Ford (1983) suggested that strike-oriented groundwater flows in pre-glacial Canadian Rocky Mountains underlain by sedimentary rocks. The results of these previous studies support the idea of major groundwater flow along bedding planes in sedimentary rock mountains, which is consisted with our findings based on the study of the twelve headwater catchments.

In this study, opposite dip-oriented catchments were classified as QSF, and dip-oriented catchments were classified into the DSF. The TWI distributions shown in Figure 10 could not be used to explain these differences in runoff characteristics. According to Beven and Kirkby (1979), TWI can be used to explain the frequency of the generation of saturation-excess overland flow. The runoff properties of overland flow are primarily affected by topographical slope values, i.e., a steeper slope accelerates overland flow runoff. Table II shows that the catchments classified as QSF (*i.e.,* catchments S05, S06, and S07) had an average slope of ∼40°, while those classified as DSF (*i.e.,* catchments S10, S11, and S12) had an average slope of ∼38°.

Figure 12, which shows detailed slope analyses, revealed the relationship between the upstream area and the topographical slope for each of 1 × 1 m grids located in each catchment. Given that the raw data showed wide scatter, this figure shows the running average of the slope and area values, which were calculated using the neighboring 300 data with respect to the upstream area. To discuss overland flow movements, slope values with small upstream areas should be neglected. If we focus on the slope value in the region where the upstream slope area is greater than 400 m^2, the slope angles of the QSF catchments will be greater than those of the DSF catchments. Thus, slope angles could be one of the main factors that can be used to describe the differences between the runoff responses of QSF and DSF catchments, i.e., the opposite dip-oriented catchments have steeper topography, which resulted in the quicker storm flow generation, while the dip-oriented catchments have gentler topography, which resulted in the more delayed storm flow generation.

Ford (1983) and Yeh, Chan, Chang, Lin, and Hsieh (2014) reported that in sedimentary rock mountains, the differences in the erosion resistance of each of the deposited layers result in the development of a landform called cuesta, where the slope is gentle on dip sides and steep on opposite dip sides. This trend has been reported in several studies (Aramaki *et al.*, 1984; Suzuki & Nakanishi, 1990; Iwahashi, Sato, & Yamagishi, 2006; Yagi, Yamasaki, & Atsumi, 2007). Thus, the differences in the slope angles of the dip-oriented and opposite dip-oriented catchments shown in Figure 12 are probably typical of many sedimentary rock mountains.

As shown in Figure 12, the strike-oriented catchments, S03 and S09, have relatively small slope angles. This probably resulted in the restricted increases in storm peak discharge, resulting in a drop in Q_i^* values during the storm events (Figures 6, 7, and S1).

Our findings in this study are supported by some previous studies such as Jencso and McGlynn (2011) and Payn, Gooseff, McGlynn, Bencala and Wondzell (2012). Both studies are conducted in the Tenderfoot Creek Experimental Forest (TCEF), located in central Montana, USA. The bedrock of TCEF is sedimentary rocks, partially including quartz monzonite. These studies concluded that topography is the main factor affecting storm flow, whereas subsurface structure is the dominant factor influencing baseflow generations.

A summary of the effects of geological structures on rainfall-runoff responses in sedimentary rock mountains is shown in Figure 13. The effect of the geological structures could be attributed to the different classes of the catchments, i.e., strike-oriented, dip-oriented, and opposite dip-oriented catchments. In strike-oriented catchments, a significant quantity of groundwater, which flowed along the bedding plane owing to hydraulic anisotropy, exfiltrated and sustained the large amount of baseflow. Thus, the geological structure had a direct influence on the runoff characteristics of strike-oriented catchments. For dip-oriented and opposite dip-oriented catchments, the difference in geological structures resulted in surface topography differences. The slopes associated with dip-oriented catchments were found to be gentler than those associated with opposite dip-oriented catchments. This resulted in delayed storm flow occurrence in dip-oriented catchments and in quick storm flow occurrence in opposite dip-oriented catchments. Therefore, even though surface topography directly controls rainwater discharges in dip-oriented and the opposite dip-oriented catchments, differences in runoff characteristics are basically attributed to geological structures.

CONCLUSION

By investigating rainfall-runoff responses at twelve catchments that extend radially from the peak of Mt. Kanayama, which is underlain by sedimentary rocks, it was found that the catchments could be classified under three groups as characterized by large baseflow (LBF), quick storm flow (QSF), and delayed storm flow (DSF). These groups were analyzed by focusing on the relationship between flow directions and geological structures based on the dips and strikes typical of sedimentary rocks. The results obtained showed that LBF, QSF, and DSF catchments corresponded to catchments with flow directions oriented toward the strike, opposite dip, and dip directions, respectively.

In the strike-oriented catchments, the runoff characteristics were directly controlled by the geological structures, i.e., owing to the hydraulic anisotropy of the sedimentary rocks, large quantities of groundwater flowed along bedding planes, sustaining the large amount of baseflow discharge. On the other hand, based on the geological structures, the opposite dip-oriented catchments have slopes that are steeper slope than those of the dip-oriented catchments. Thus, the opposite dip-oriented catchments were characterized by quick storm flow, while the dip-oriented catchments showed delayed storm flow. These findings indicate that in dip-oriented and opposite dip-oriented catchments, runoff characteristics are indirectly controlled by the geological structures.

Therefore, in this study, the effects of geological structures on rainfall-runoff responses in headwater catchments located in sedimentary rock mountains were clarified. Future research should focus on the hydrological processes in each catchment by conducting detail analyses of topographical effects on storm discharge hydrographs and identifying bedrock groundwater flow pathways.

REFERENCES

Aramaki S, Kitazono Y, Nakayama H, Suzuki A, & Kaziwara M. 1984. On the Hazard Map of Slope Failure of Landslide-type in Amakusa Islands, Kumamoto Prefecture. *Journal of the Japan Society of Engineering Geology 25*(2) pp.47-58 (in Japanese with English abstract).

Beven K. 2002. Hydrological Similarity and distribution Function Rainfall-Runoff Models. *Rainfall- Runoff Modelling The Primer* pp.179-216. John Willey & Sons.

Beven K, & Kirkby M. 1979. A physically based, variable contributing area model of basin hydrology. *Hydrological Sciences Journal 24*(1) pp.43-69.

Bruno M. 1994. Micromechanics of stress-induced permeability anisotropy and damage in sedimentary rock. *Mechanisc of Materials 18* pp.31-48.

Burns D, Murdoch P, Lawrence G, & Michel R. 1998. Effect of groundwater springs on NO_3^- concentrations during summer in Catskill Mountain streams. *Water Resources Research 34*(8) pp.1987-1996.

Corominas J, Moya J, Ledesma A, Lloret A, & Gili J. 2005. Prediction of ground displacements and velocities from groundwater level changes at the Vallcebre landslide (Eastern Pyrenees, Spain). *Landslides 2* pp.83-96.

Ford D. 1983. Alpine Karst Systems at Crowsnest Pass, Alberta-British Columbia, Canada. *Journal of Hydrology 61* pp.187-192.

Fujimoto M, Ohte N, & Tani M. 2008. Effects of hillslope topography on hydrological responses in a weathered granite mountain, Japan: Comparison of the runoff response between the valley-head and the side slope. *Hydrological Processes 22* pp.2581-2594.

Han S, Yang Y, Fan T, Xiao D, & Moiwo J. 2012. Precipitation-runoff processes in Shimen hillslope micro-catchment of Taihang Mountain, north China. *Hydrological Processes 26* pp.1332-1341.

Hernandez T, Nachabe M, Ross M, & Obeysekera J. 2003. Modeling Runoff from Variable Source Areas in Humid, Shallow Water Table Environments. *Journal of the American Water Resources Association 39*(1) pp.75-85.

Hewlett J & Hibbert A. 1967. Factors Affecting the Response of Small Watersheds to Precipitation in Humid Areas. *International Symposium on Forest Hydrology* pp.275-290

Hughes D. 1995. Monthly rainfall-runoff models applied to arid and semiarid catchments for water resource estimation purposes. *Hydrological Sciences Journal 40*(6) pp.751-769.

Iwahashi J, Sato H, & Yamagishi H. 2006. The Spatial Distribution of Shallow Landslides Caused by the Mid Niigata Prefecture Earthquake in 2004 – Analyses Focusing on the Data of 1:25,000 scale Damage Maps Prepared by GSI -. *Journal of the Geospatial Information Authority of Japan 110* pp.81-89 (in Japanese).

Iwashita H, Onda Y, & Ichiyanagi K. 1994. Storm-runoff characteristics of the three small steep watersheds, upstream of the Tenryu river. *Bulletin of the Nagoya University Forests 13* pp.85-108 (in Japanese with English abstract).

Japan Meteorological Agency. Retrieved January 30, 2020, from
http://www.data.jma.go.jp/obd/stats/etrn/view/nml_amd_ym.php?prec_no=60&block_no=0964&year=&month=&day=&view=
(in Japanese).

Jefferson A, Grant G, & Rose T. 2006. Influence of volcanic history on groundwater patterns on the west slope of the Oregon High Cascades. *Water Resource Research 42* W12411 doi: 10.1029/2005WR004812.

Jencso K, & McGlynn B. 2011. Hierarchical controls on runoff generation: Topographically driven hydrologic connectivity, geology, and vegetation. *Water Resource Research 47* W11527 doi: 10.1029/2011WR010666.

Kato Y, Onda Y, Mizuyama T, Kosugi K, Yoshikawa A, Tsujimura M, … Okamoto M. 2000. The difference of runoff peak response time in upstream of Ibi River underlain by different geology. *Journal of the Japan Society of Erosion Control Engineering 53*(4) pp.38-43 (in Japanese with English abstract).

Kirkby M, Bracken L, & Reaney S. 2002. The Influence of Land Use, Soils and Topography on the Delivery of Hillslope Runoff to Channels in SE Spain. *Earth Science Processes and Landforms 27* pp.1459-1473.

Komatsu Y. 2008. Scaling and Distribution of Base Flow in Mesozoic Sedimentary Rocks Catchments, the Koto river. *Bulletin of geo-environmental science 10* pp.107-114 (in Japanese).

Kosugi K, Fujimoto M, Katsura S, Kato H, Sando Y, & Mizuyama T. 2011. Localized bedrock aquifer distribution explains discharge from a headwater catchment. *Water Resources Research 47* W07530 doi: 10.1029/2010WR009884.

López-Tarazón J, Batalla R, Vericat D, & Balasch J. 2010. Rainfall, runoff and sediment transport relations in an mesoscale mountainous catchment: The River Isábena (Ebro basin). *Catena 82* pp.23-34.

Marutani T, Kaibori M, Jitousono T, Mizuno H, Ohno H, Shimizu O, … Yamada Y. 2017. Sediment-related Disasters by a heavy Rainfall in the northern Part of Kyusyu-Island, Japan in July 2017. *Journal of the Japan Society of Erosion Control Engineering 70*(4) pp.31-42 (in Japanese with English abstract).

Miyagi T, Higaki D, Yagi H, Doshida S, Umemura J, & Satoh G. 2011. Reconnaissance report on landslide disasters in northeast Japan following the M9 Tohoku earthquake. *Landslides 8* pp.339-342.

Miyata S, Uchida T, Asano Y, Ando H, & Mizuyama T. 2003. Effects of bedrock groundwater seepage on runoff generation at a granitic first order stream. *Journal of the Japan Society of Erosion Control Engineering 56*(1) pp.13-19 (in Japanese with English abstract).

Okada N, Ye T, Kajitani Y, Shi P, & Tatano H. 2011. The 2011 Eastern Japan Great Earthquake Disaster: Overview and Comments. *International Journal of Disaster Risk Science 2* pp.34-42.

Payn R, Gooseff M, McGlynn B, Bencala K, & Wondzell S. 2012. Exploring changes in the spatial distribution of stream baseflow generation during a seasonal recession. *Water Resource Research 48* W04519 doi: 10.1029/2011WR011552.

QGIS Development Team (2019). *QGIS Geographic Information System*. Open Source Geospatial Foundation Project. http://qgis.osgeo.org

Sakai R, Munakata M, & Kimura H. 2009. Methodological studies for evaluation of groundwater flow system in a sedimentary rock area: Case study for the Boso Penisula. *Journal of Groundwater Hydrology 51*(4) pp.311-329 (in Japanese with English abstract).

Séguis L, Kamagaté B, Favreau G, Descloitres M, Seidel J, Galle S, …, Wubda M. 2011. Origins of streamflow in a crystalline basement catchment in a sub-humid Sundanian zone: The Donga basin (Benin, West Africa) Inter-annual variability of water budget. *Journal of Hydrology 402* pp.1-13.

Sekhon J. 2011. Multivariate and Propensity Score Matching Software with Automated Balance Optimization: The Matching Package for R. *Journal of Statistical Software 42*(7) pp.1-52.

Singhal B & Gupta R. 2010. Hydraulic properties of Rocks. *Applied Hydrogeology of Fractured Rocks* pp.139-154. Springer Science+Business Media B. V.

Suenaga H, Kiho K, & Okada T. 2002. An Evaluation for Permeability Anisotropy of Sedimentary Rock by Labolatory Experiment. *Journal of the Japan Society of Engineering Geology 43*(5) pp.284-292 (in Japanese with English abstract).

Suzuki M. 1980. Evaporation from a Small Catchment in Hilly Mountains (I) Seasonal Variations in Evapotranspiration, Rainfall Interception and Transpiration. *Journal of the Japanese Forest Society 62*(2) pp.46-53.

Suzuki T & Nakanishi A. 1990. Rates of Decline of Fluvial Terrace Scarps in the Chichibu Basin, Japan. *Transactions, Japanese Geomorphological Union 11*(2) pp.117-149.

Tani M, Fujimoto M, Katsuyama M, Kojima N, Hosoda I, Kosugi K, … Nakamura S. 2012. Predicting the dependencies of rainfall-runoff responses on human forest disturbances with soil loss based on the runoff mechanisms in granite and sedimentary rock mountains. *Hydrological Processes 26* pp.809-826.

Uchida T, Kosugi K, & Mizuyama T. 1999. Runoff characteristics of pipeflow and effects of pipeflow on rainfall-runoff phenomena in a mountainous watershed. *Journal of Hydrology 222* pp.18-36.

Ushiyama M, Honma M, Yokomaku S, & Sugimura K. 2019. Characteristics of victims caused by heavy rainfall disaster in July, 2018. *Journal of Japan society for Natural disaster Science 38*(1) pp.29-54 (in Japanese with English abstract).

Wakita K, Takeuchi T, Mizuno K, Komatsubara T, Nakano S, Takemura K, & Taguchi Y. 2013. Geological Map of Japan 1:50,000, Kyoto-Tonambu. Geological Survey of Japan, AIST.

Yagi H, Yamasaki T, & Atsumi M. 2007. GIS analysis on geomorphological features and soil mechanical implication of landslides caused by 2004 Niigata Chuetsu earthquake. *Journal of the Japan Landslide Society 43*(5) pp.294-306 (in Japanese with English abstract).

Yeh C, Chan Y, Chang K, Lin M, & Hsieh Y. 2014. Derivation of Strike and Dip in Sedimentary Terrain Using3D Image Interpretation Based on Airborne LiDAR Data. *Terrestrial, Atmospheric and Oceanic Sciences 25*(6) pp.775-790.

Zevenbergen L, & Thorne C. 1987. Quantitative analysis of Land Surface Topography. *Earth surface Processes and Landforms 12* pp.47-56.

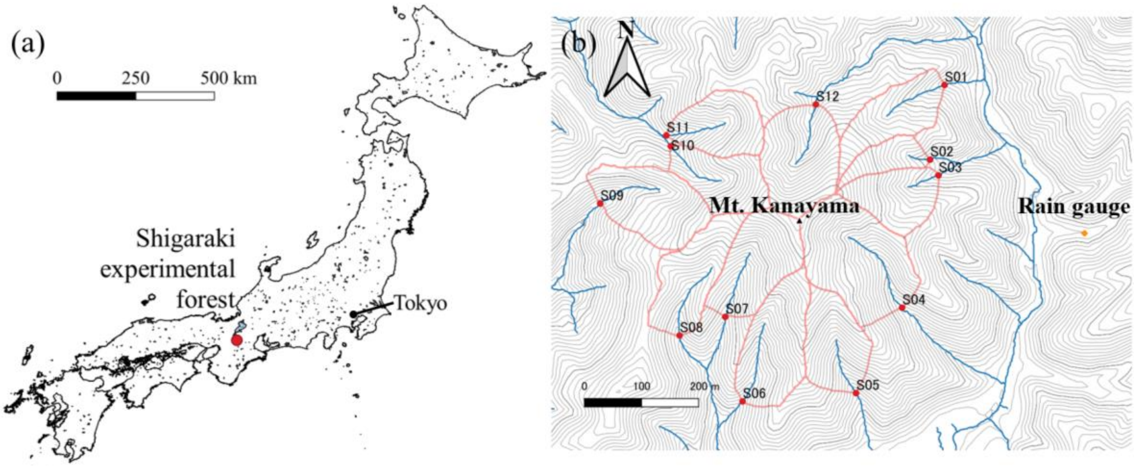

Figure 1. (a) Location and (b) Topography of the study site. The grey contours are located at 5-m intervals, while the black contours are located at 50-m intervals. Channels are drawn for locations with 5,000 m^2 or larger upstream areas.

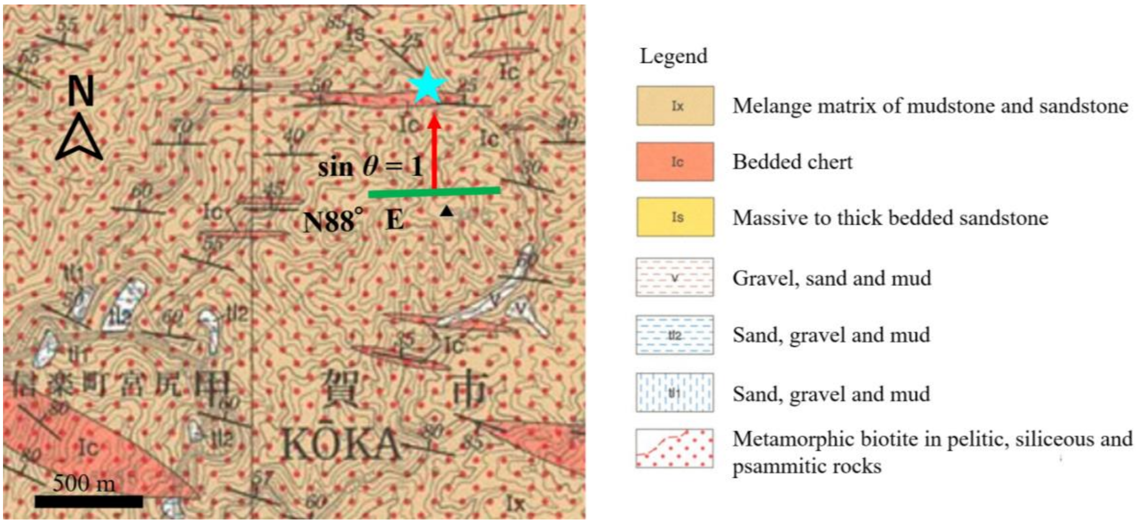

Figure 2. Geological map of the study area, including the N88° E line and the arrow perpendicular to the N88° E line shown in Figure 8. The light blue star indicates the location of the slope shown in Figure 3. The green line, red arrow, light blue star, summit mark, scale bar, compass mark, and North mark were added to the geological map produced by Wakita *et al*. (2013).

Figure 3. Dips and strikes in the study area. This picture was taken at the place indicated by the light blue star in Figure 2. In this picture, the strike is N83° E and the dip is 65° N.

Table I. Average dip value and strike direction in the vicinity of the study site.

Source	Points	Dip	Strike
Wakita *et al.* (2013)	8	39° N	N100.7° E
Our research	35	59° N	N101.8° E
Average	43	55° N	N101.6° E

Table II. Catchment areas and average slopes.

Catchments	Area [ha]	Average slope [°]
S01	1.53	32.2
S02	0.696	35.1
S03	1.37	35.4
S04	3.08	39.4
S05	1.63	40.6
S06	2.15	40.2
S07	2.01	39.2
S08	1.83	34.0
S09	2.13	35.1
S10	1.44	37.8
S11	1.47	38.1
S12	2.19	37.6

Table III. Characteristics of rainfall events.

Event	Date	Total rainfall [mm]	Peak intensity [mm/10min.] ([mm/h])	No-precipitation period before event
1	24 Sep 2014 22:20- 25 Sep 2014 5:40	57.5	6.5 (21.5)	13 days 7 hours 10 minutes
2	5 Oct 2014 13:20- 6 Oct 2014 13:20	62.5	3.5 (14.5)	10 days 7 hours 50 minutes

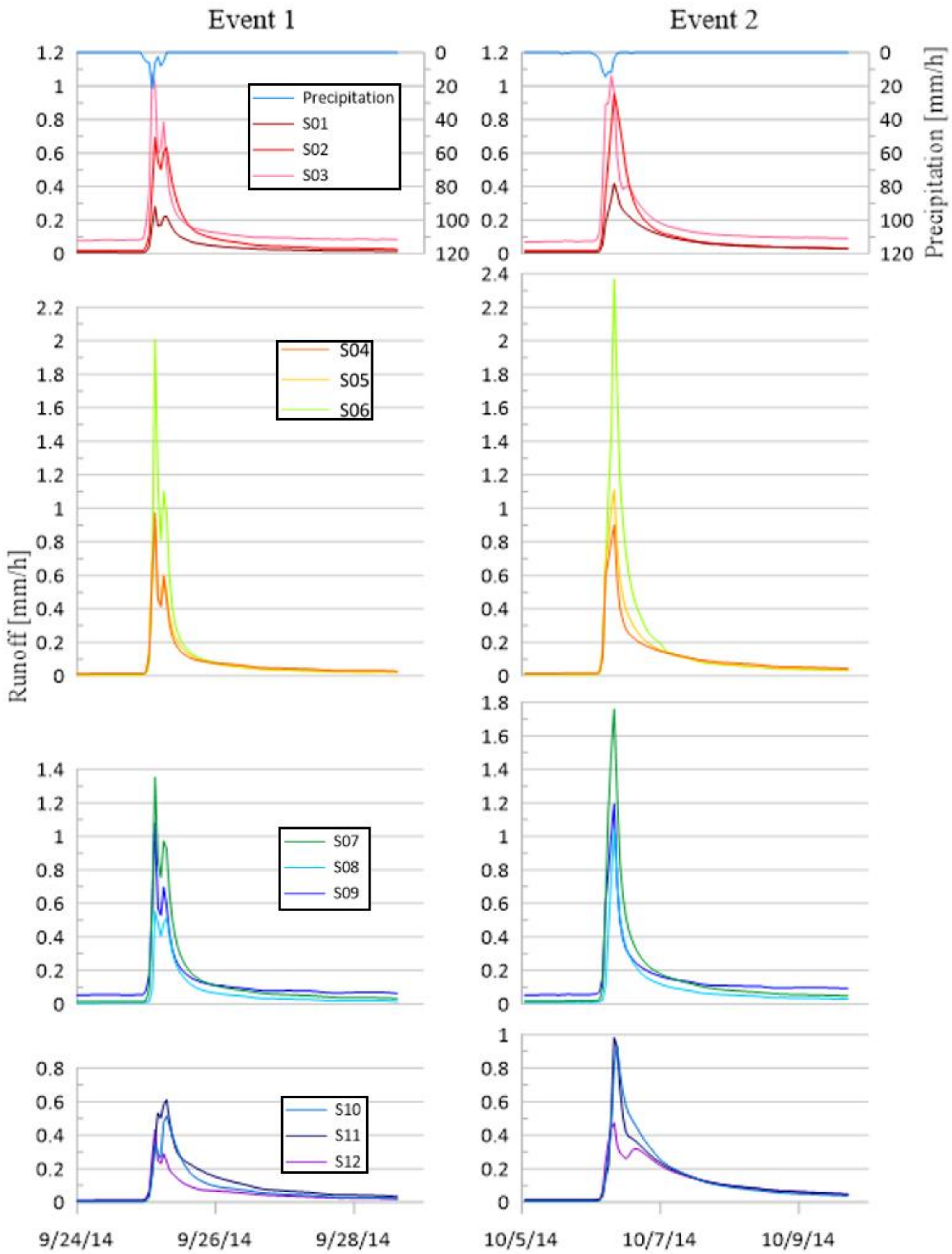

Figure 4. Observed hyetographs and hydrographs for the events 1 and 2.

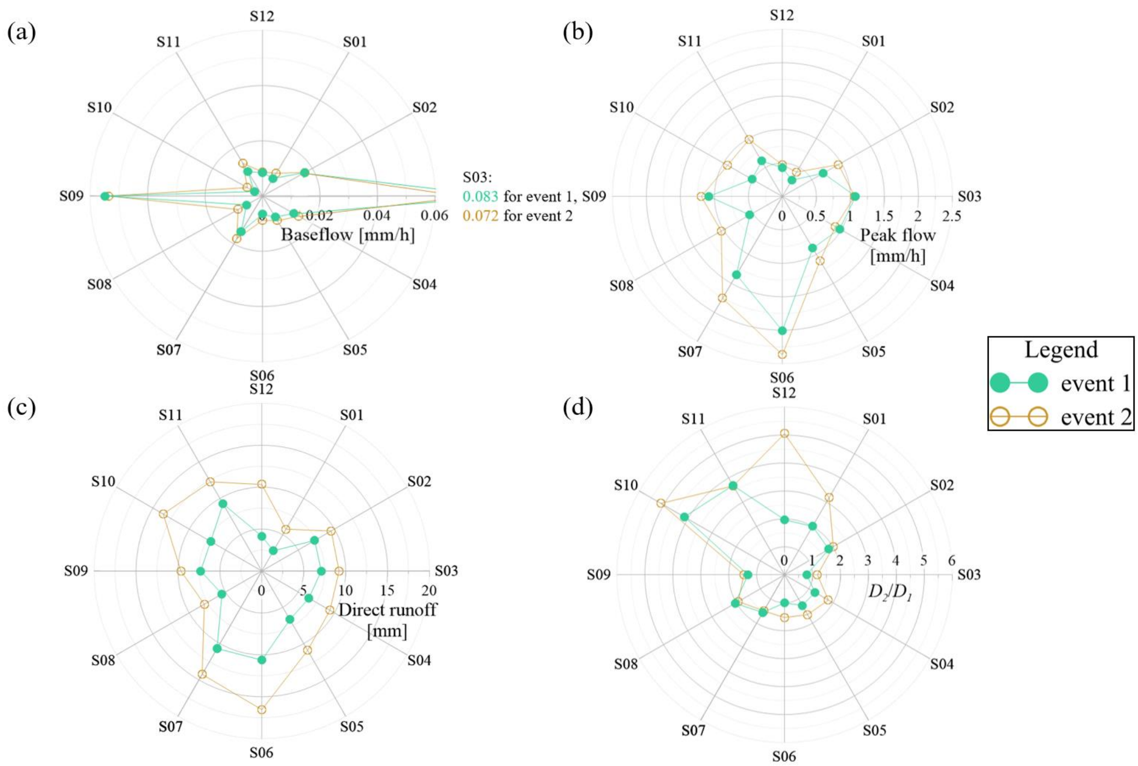

Figure 5. Characteristics of the studied two storm events showing (a) baseflow rate just before each event, (b) peak flow rate, (c) amount of direct runoff, and (d) ratio of D_2 to D_1 where D_1 represents direct runoff amount during the period from the start to the end of precipitation, and D_2 represents the direct runoff amount for 24 hours just after precipitation ceased.

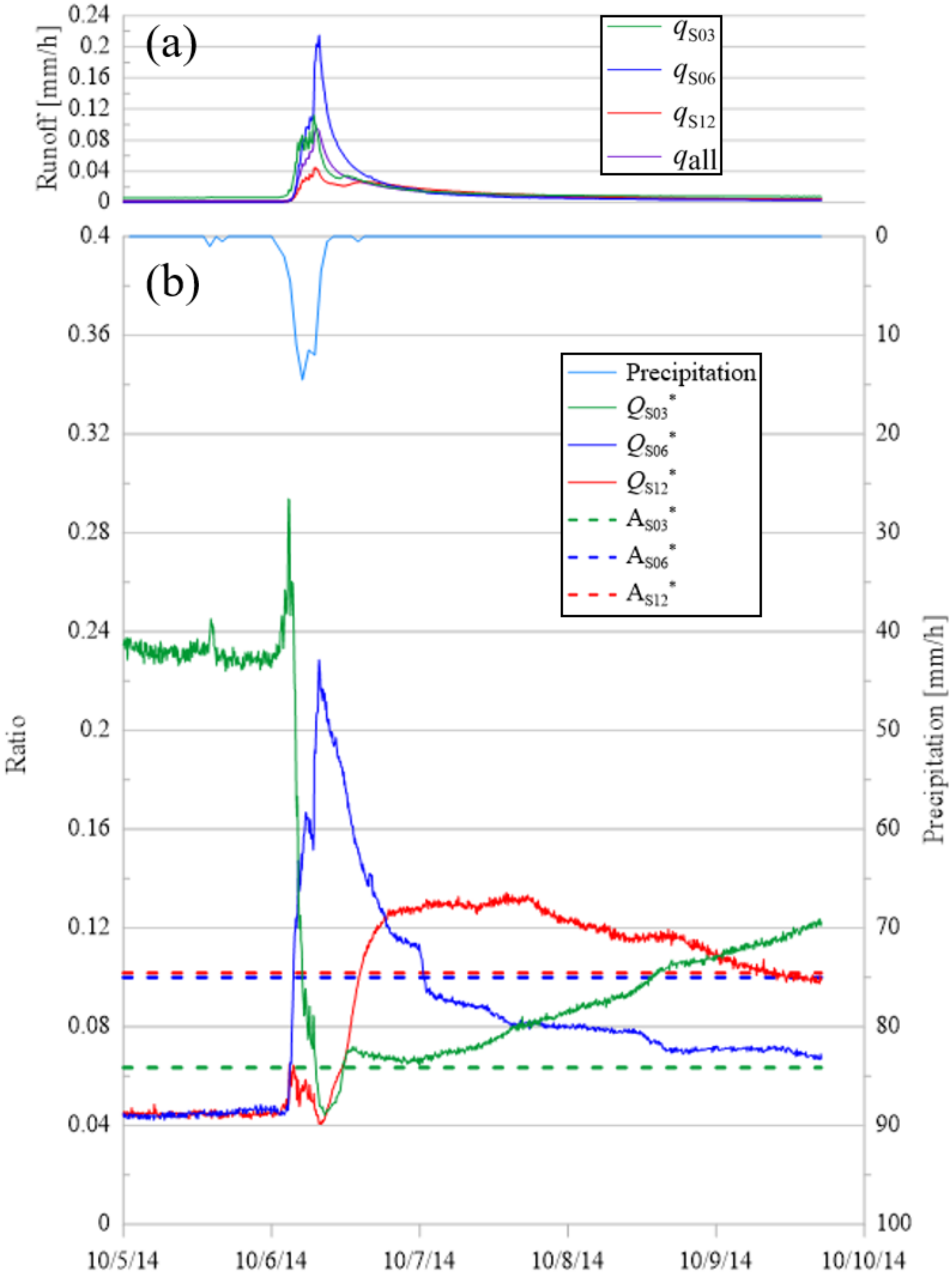

Figure 6. (a) Specific discharge q_i, and (b) Area-proportional discharge ratio, A_i^*, and the observed discharge ratio, Q_i^*, for catchments S03, S06, and S12 (event 2). In Figure 6(a), the total specific discharge from the mountain, q_{all}, is included. In Figure 6(b), the hourly precipitation is included. Note that A_{S06}^* and A_{S12}^* are about the same value.

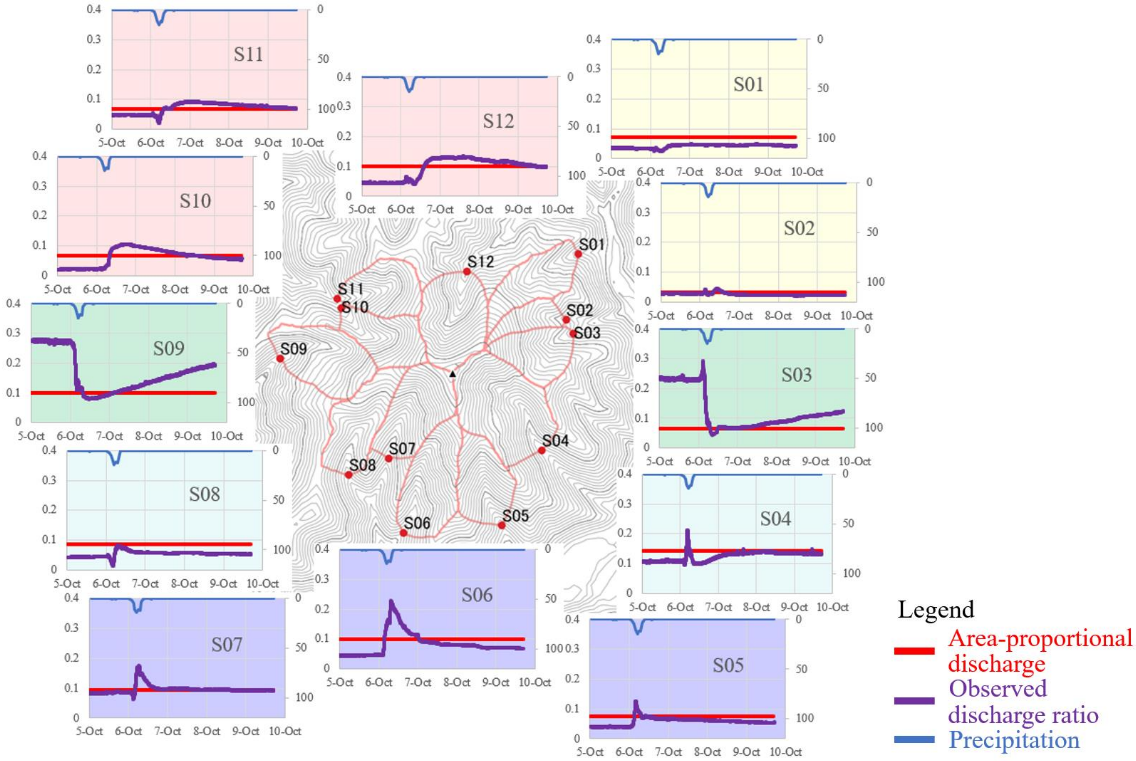

Figure 7. Variation of A_i^* and Q_i^* for the event 2. In each panel, the left axis represents the discharge ratio, and the right axis represents precipitation [mm/h].

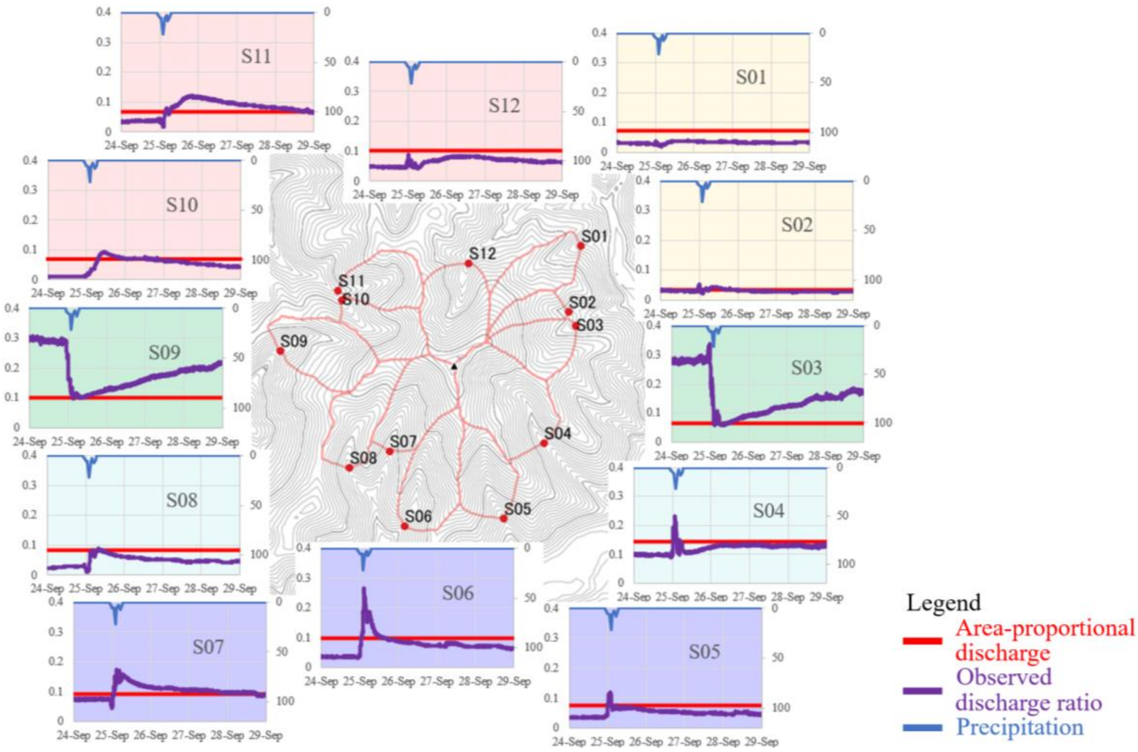

Figure S1. Variation of A_i^* and Q_i^* for event 1. The axes are as defined in Figure 7.

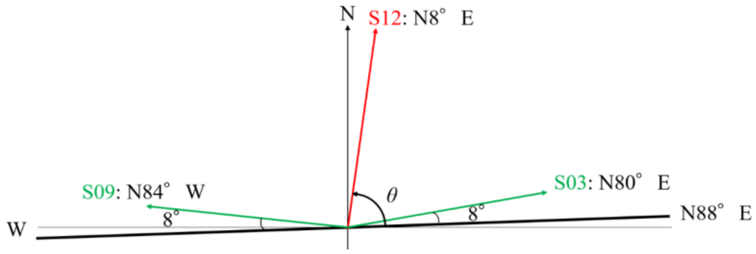

Figure 8. Flow directions for catchments S03, S09, and S12, along with the defined θ. The flow directions for catchments S03 and S09, both of which were categorized as LBF catchments, are oriented northward by 8° from the N88° E line. The flow direction of S12 is shown as an example for sin θ calculation.

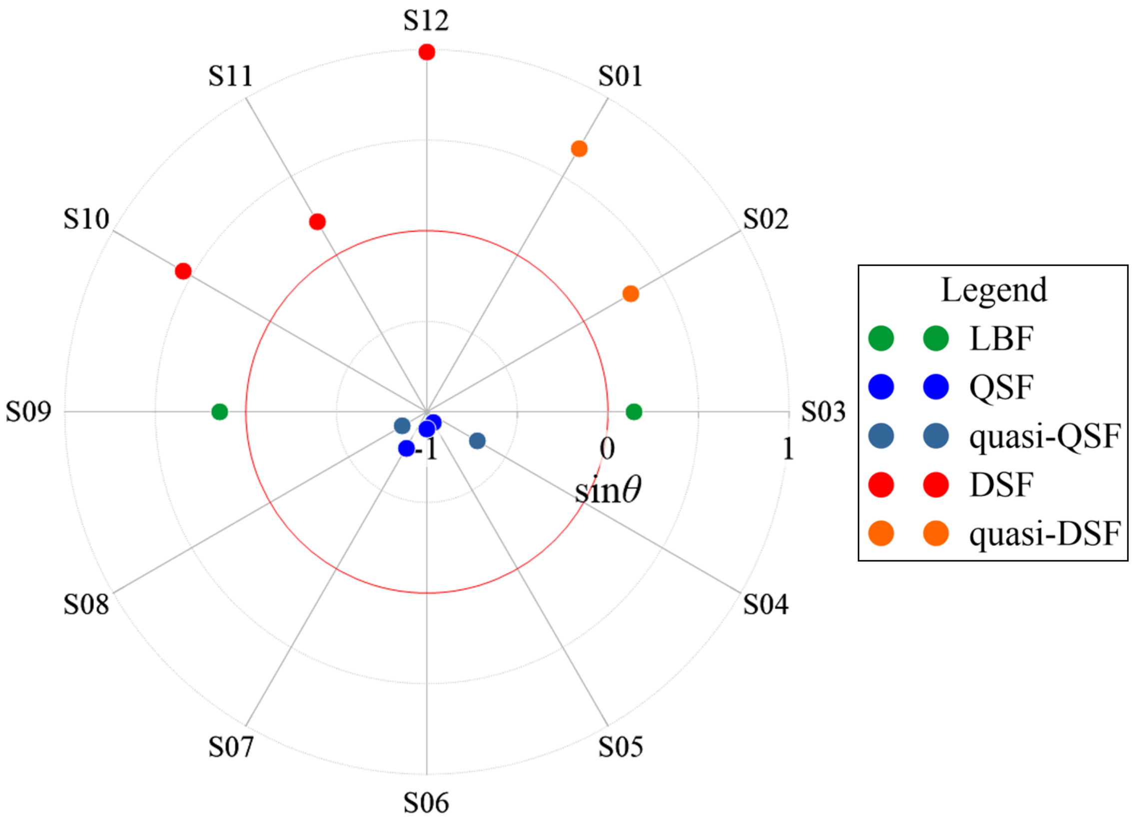

Figure 9. Sin θ for the different catchments. Sin θ is defined in Figure 8. The acronyms in the legend represent catchment classification.

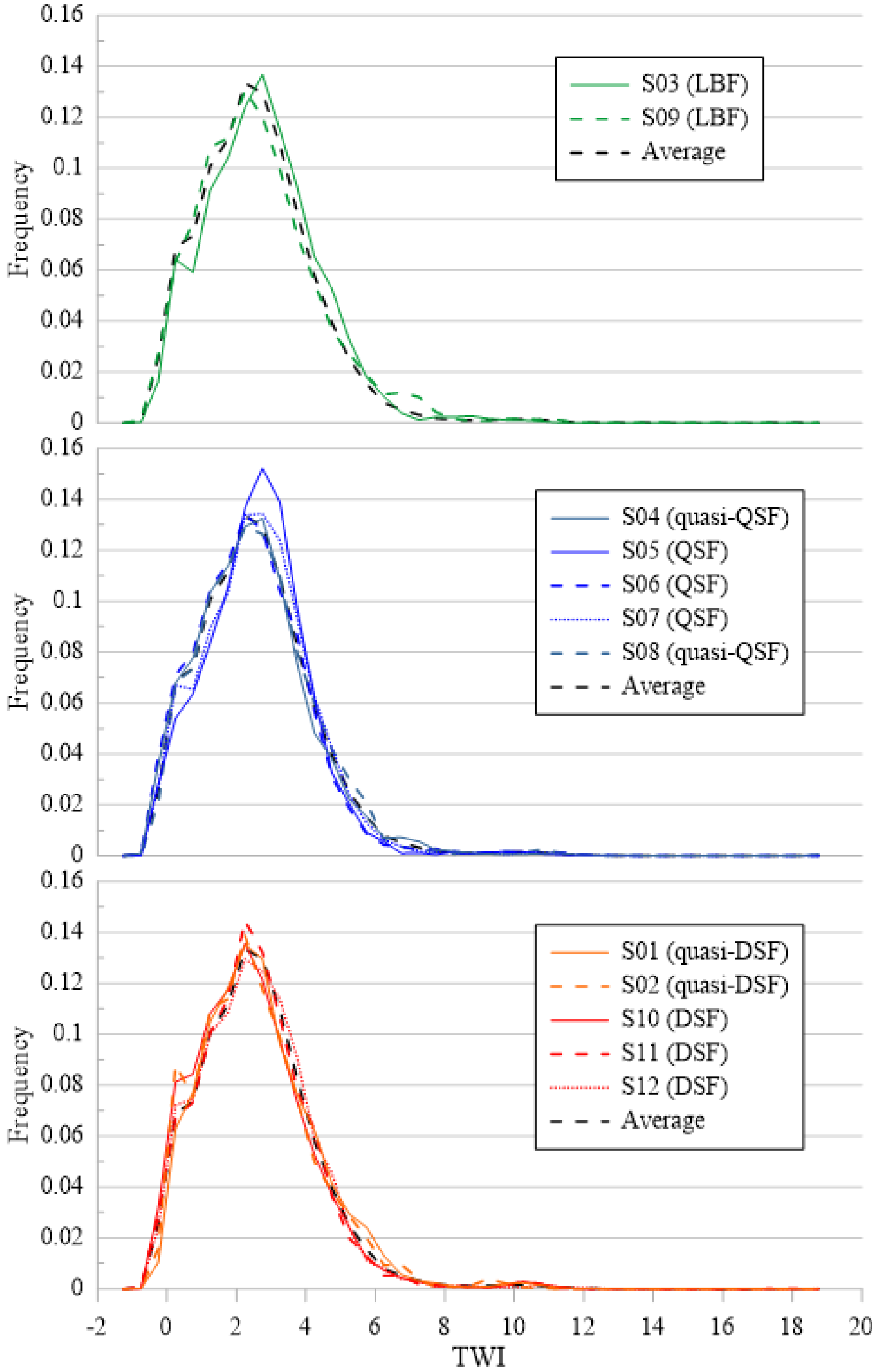

Figure 10. Distribution of TWI (topographic wetness index) for each catchment. The black dotted lines represent TWI distribution for all the 12 catchments. The class interval is 0.5.

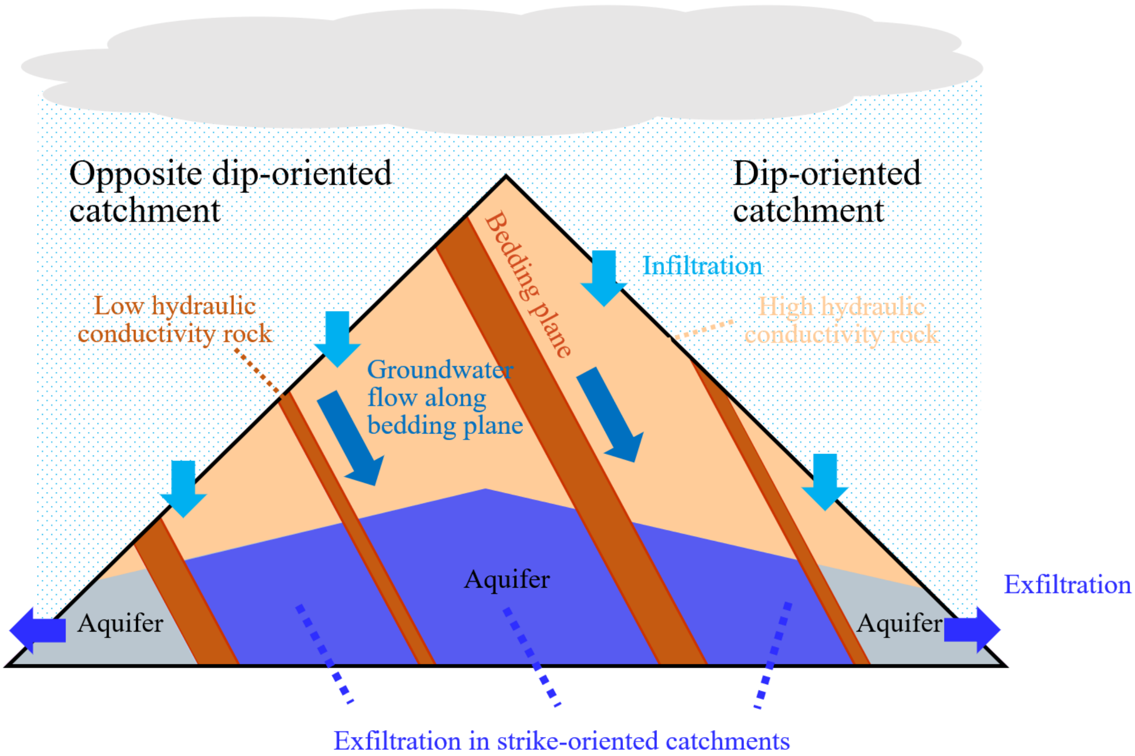

Figure 11. Cross section image of the study site. The figure shows geological stratigraphy consisting of high and low hydraulic conductivity rocks, distribution of bedrock aquifer, and water flow pathways.

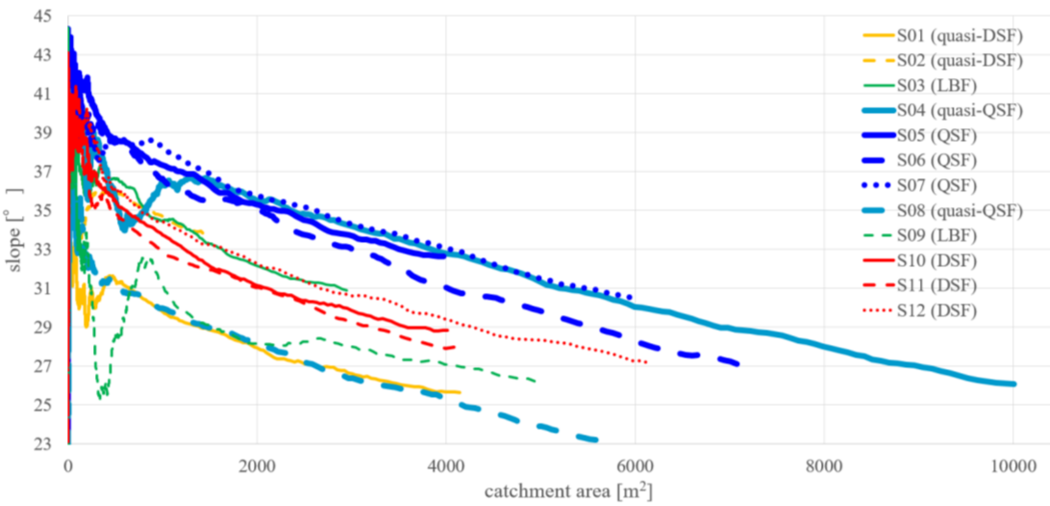

Figure 12. Relationship between slope angle and catchment area for each catchment, showing running average values for neighboring 300 data with respect to the catchment area. Slope angles and catchment area were calculated by using SAGA plugins from QGIS (ver. 3.4.12) (QGIS Development Team, 2019).

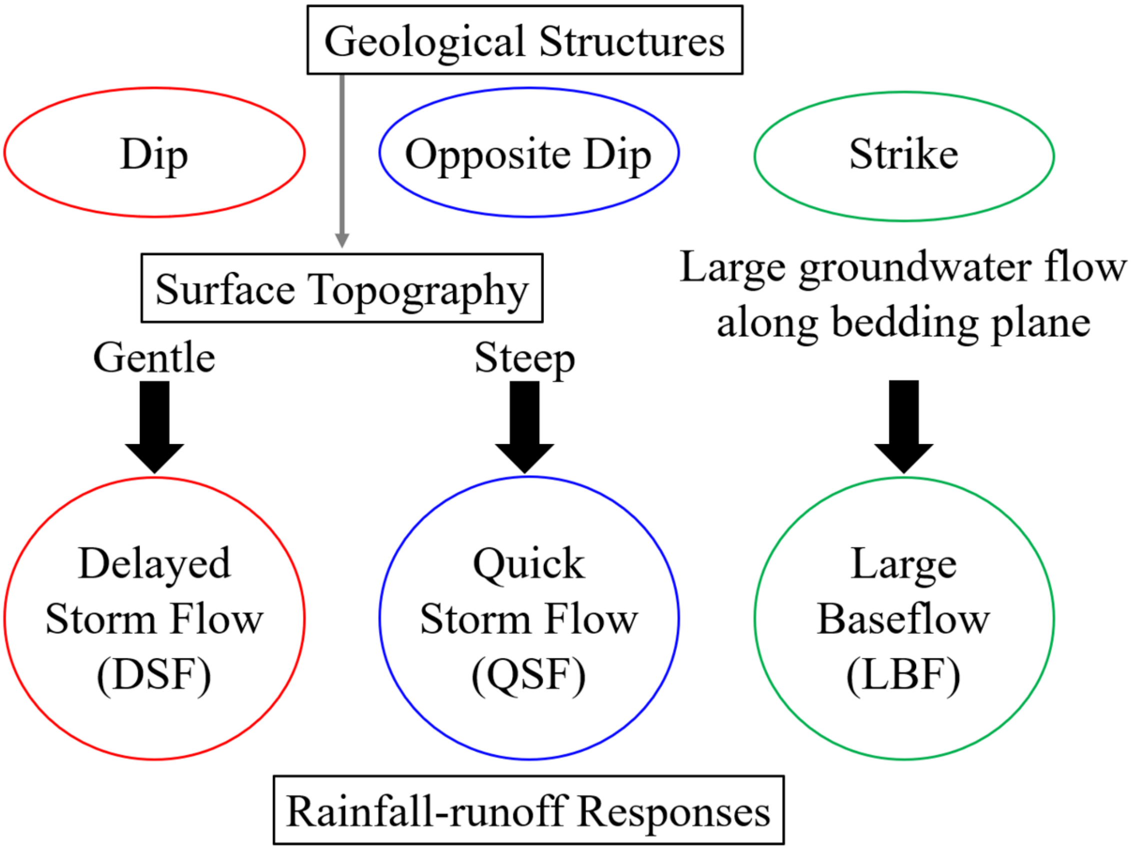

Figure 13. Effects of geological structures on the rainfall-runoff responses of the sedimentary rock mountain studied.